Highly efficient organic light-emitting diodes with hole injection layer of transition metal oxides

Soo Young Kim, Jeong Min Baik, Hak Ki Yu, and Jong-Lam Lee

Articles you may be interested in

Efficient and reliable green organic light-emitting diodes with Cl2 plasma-etched indium tin oxide anode
J. Appl. Phys. **112**, 013103 (2012); 10.1063/1.4731713

Enhancement of optical properties in organic light emitting diodes using the Mg–Al alloy cathode and Ir O x -coated indium tin oxide anode
Appl. Phys. Lett. **88**, 112106 (2006); 10.1063/1.2179108

Effect of thin iridium oxide on the formation of interface dipole in organic light-emitting diodes
Appl. Phys. Lett. **87**, 232105 (2005); 10.1063/1.2135874

Rhodium-oxide-coated indium tin oxide for enhancement of hole injection in organic light emitting diodes
Appl. Phys. Lett. **87**, 072105 (2005); 10.1063/1.2012534

Enhancement of hole injection using O 2 plasma-treated Ag anode for top-emitting organic light-emitting diodes
Appl. Phys. Lett. **86**, 012104 (2005); 10.1063/1.1846149

Highly efficient organic light-emitting diodes with hole injection layer of transition metal oxides

Soo Young Kim, Jeong Min Baik, Hak Ki Yu, and Jong-Lam Lee[a)]
*Department of Materials Science and Engineering, Pohang University of Science and Technology
(POSTECH), Pohang, Kyungbuk 790-784, Korea*

We report on the advantage of interlayers using transition-metal oxides, such as iridium oxide (IrO_x) and ruthenium oxide (RuO_x), between indium tin oxide (ITO) anodes and 4′-bis[N-(1-naphtyl)-N-phenyl-amino]biphenyl (α-NPD) hole transport layers on the electrical and optical properties of organic light-emitting diodes (OLEDs). The operation voltage at a current density of 100 mA/cm^2 decreased from 17 to 11 V for OLEDs with 3-nm-thick IrO_x interlayers and from 17 to 14 V for OLEDs with 2-nm-thick RuO_x ones. The maximum luminance value increased about 50% in OLED using IrO_x and 108% in OLED using RuO_x. Synchrotron radiation photoelectron spectroscopy results revealed that core levels of Ru 3d and Ir 4f shifted to high binding energies and that the valence band was splitting from metallic Fermi level as the surface of the transition metal was treated with O_2 plasma. This provides evidence that the transition-metal surface transformed to a transition-metal oxide. The surface of the transition metal became smoother with the O_2 plasma treatment. The thickness was calculated to be 0.4 nm for IrO_x and 0.6 nm for RuO_x using x-ray reflectivity measurements. Secondary electron emission spectra showed that the work function increased by 0.6 eV for IrO_x and by 0.4 eV for RuO_x. Thus, the transition-metal oxides lowered the potential barrier for hole injection from ITO to α-NPD, reducing the turn-on voltage of OLEDs and increasing the quantum efficiency. © *2005 American Institute of Physics.* [DOI: 10.1063/1.2123375]

I. INTRODUCTION

Ever since the highly efficient organic light-emitting diode (OLED) was reported, numerous efforts have been undertaken to improve the OLED characteristics. The performance of an OLED was influenced by injecting electrode properties and electrode-organic interfaces.[1] The potential barrier between electrodes and organic layers exists due to the energy-level difference. To reduce the operation voltage and increase the luminance efficiency, energy barriers at the organic material interface with electrodes should be reduced.

For the injection of electrons, it is desirable to use metals with low work functions in the cathode region. Such metals are always susceptible to atmospheric oxidation. Aluminum (Al) has been widely used as a cathode for OLEDs due to its better oxidation resistance and ease-of-manufacturing properties. However, Al is not suitable for low-voltage-operated OLEDs due to its relatively high work function (4.28 eV).[2] Therefore, a thin insulating interlayer, such as LiF, SrO_x, NaCl, and NaSt ($C_{17}H_{35}COONa$), has been used between the Al cathodes and the emitting materials to generate interfacial dipoles that result in favorable alignment of cathode Fermi levels and the lowest unoccupied molecular orbital (LUMO) energy levels of the electron transport layer.[3–6] The barrier against electron emission is subsequently reduced.

For the injection of holes, indium tin oxide (ITO) has been used as the most common OLED anode due to its high transparency, high conductivity, and high work function.[7] At the interface of ITO anodes with organic materials, such enhanced hole injection was also desired in order to increase the internal quantum efficiency by balancing charge carriers in the active layer. In order to reduce the potential barrier for hole injection, it was effective to treat the surface of ITO with an appropriate surface treatment, such as ultraviolet ozone cleaning, argon ion bombardment, or atmospheric plasma exposure.[8–10] These treatments were effective in removing the residual surface contaminants and increasing oxygen content at the ITO surface, leading to the increase of work function. Even though such treatments were applied to the ITO surface, the ITO work function was not high enough to reduce the potential barrier for hole injection. And several kinds of approaches have been proposed to elevate the work function of ITO, such as using metal oxides with high work functions, inserting conducting polymers between ITO and organic material, and depositing metal-doped ITO layers on the ITO surface.[11–13] Iridium oxide (IrO_x) and ruthenium oxide (RuO_x) are transparent conducting oxides. The work functions of IrO_x and RuO_x (>5.0 eV) are higher than those of ITO (~4.7 eV).[14] Thus, it is expected that using IrO_x or RuO_x as a hole injection layer (HIL) between ITO anodes and organic materials could enhance the electrical properties of OLED via improvement of hole injection.

In this paper, we report the enhancement of electrical and optical performance of OLEDs by inserting transition-metal oxides such as IrO_x or RuO_x between ITO anodes and the hole transport layer of 4′-bis[N-(1-naphtyl)-N-phenyl-amino]biphenyl (α-NPD). The oxide layers were prepared by exposing the thin transition-metal layers to O_2 plasma. The change in the work function with oxide forma-

[a)]Electronic mail: jllee@postech.ac.kr

tion was examined using synchrotron radiation photoelectron spectroscopy (SRPES). Root-mean-square (rms) value and uniformity after deposition of transition-metal layers were examined using atomic force microscopy (AFM). The x-ray reflectivity method was employed to examine the relative roughness and thickness of thin transition metal. From this, the effects of IrO_x and RuO_x on the enhancement of electrical and optical properties in OLEDs are discussed.

II. EXPERIMENT

A glass coating with ITO (150 nm thick, ∼20 Ω/□) was used as the starting substrate. The ITO surface was cleaned in sequence with acetone, isopropyl alcohol and de-ionized water, and then dried with a high-purity nitrogen gas. The ITO surface was treated with O_2 plasma for 1 min under 100 mTorr. The plasma power was 150 W. Thin layers of Ir or Ru with thicknesses of 1, 2, 3, and 4 nm was deposited on the plasma-treated ITO using a rf magnetron sputter. The thickness of the thin layer was deduced from the period of the oscillations in x-ray reflection, measured at the 3C2 beam line of the Pohang Acceleration Laboratory (PAL). The Ir and Ru films were also exposed to the O_2 plasma for 1 min to produce a IrO_x and RuO_x layer. These samples were loaded into a thermal evaporator and α-NPD with a thickness of 70 nm, tris(8-hydroxyquinoline) aluminum (Alq_3, 60 nm), and aluminum (Al, 150 nm) layers were deposited in sequence. During deposition, the base pressure of the chamber was maintained as low as 10^{-6} Torr. The active area of the device was 3×3 mm^2. The current-density voltage and luminance-current-density characteristics of the devices were measured.

AFM measurements were carried out to evaluate the rms roughness of the samples. X-ray reflectivity was used to measure the exact thickness of the Ir or Ru layers and the surface morphology change after O_2 plasma treatment. Three types of samples were prepared to investigate the change of chemical bonding states after deposition of transition-metal layers on ITO. The first sample was O_2 plasma-treated ITO (*ITO*). The second was a thin layer of Ir or Ru deposited on *ITO* (Ir/*ITO* or Ru/*ITO*). The third was O_2 plasma-treated Ir or Ru (O_2-Ir/*ITO* or O_2-Ru/*ITO*). The samples were loaded into a vacuum chamber equipped with an electron analyzer, at the 2B1 beam line in the PAL. An incident photon energy of 650 eV was used to obtain Ir $4f$, Ru $3d$, In $3d$, Sn $3d$, O $1s$, and C $1s$ core-level spectra. The onset of photoemission, corresponding to the vacuum level at the surface was measured with a negative bias (−20 V) on the sample to avoid the detector work function. The incident photon energy was calibrated with a core-level spectrum of Au $4f$.

III. RESULTS

A. Electrical and optical properties of OLEDs

Figure 1(a) shows the current-density-voltage characteristics of the three types of devices. Devices without HIL require a drive voltage of approximately 17 V to generate a current density of 100 mA/cm^2, substantially higher than that for devices with O_2-plasma-treated Ru layers (14 V) or O_2-plasma-treated Ir layers (11 V). Luminance-current-
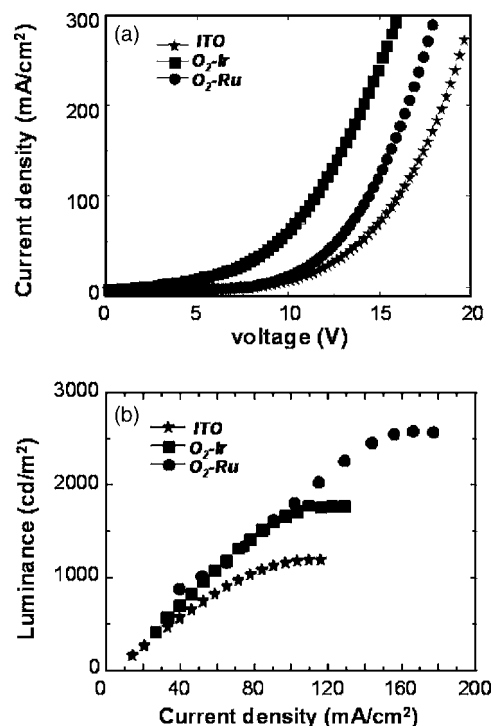

FIG. 1. (a) Current-density voltage and (b) luminescence-current-density characteristics of OLEDs with different anodes.

density curves are presented in Fig. 1(b). In all samples, the luminance value increased with current density. The maximum luminance value in *ITO* was 1200 cd/m^2, but it increased to 1800 cd/m^2 for O_2-Ir/*ITO* and 2500 cd/m^2 for O_2-Ru/*ITO*. The luminous efficiency as a function of applied current density is shown in Table I. It is thought that holes were effectively injected from anodes to organic layers, promoting internal quantum efficiency. It is considered that holes were effectively injected from anodes to organic layers as O_2-plasma-treated Ir and Ru layers were used as HIL in OLEDs, leading to the elevation of internal quantum efficiency.

Figure 2(a) shows the current density-voltage curves as a function of different Ir layer thicknesses. The electrical performance in OLEDs with O_2-plasma-treated Ir layers was enhanced in comparison with that in OLEDs without HIL. Of particular note, OLEDs with 3-nm-thick Ir layers required a drive voltage of 10 V to generate a current density of 100 mA/cm^2, which is lower by 7 V than that for devices without Ir layers. The light output spectrum as a function of different Ir layer thickness is shown in Fig. 2(b). The maximum intensity is located at the wavelength of 520 nm. It was found that the light output intensity decreased with Ir layer

TABLE I. Luminous efficiency as a function of applied current density.

Current density (mA/cm^2)	ITO (cd/A)	O_2-Ir (cd/A)	O_2-Ru (cd/A)
38.26	1.53	1.88	2.35
63.77	1.45	1.88	2.12
89.28	1.29	1.82	1.93
127.55	1.01	1.40	1.78

FIG. 2. (a) Current-density voltage and (b) light output spectrum of OLEDs with different thicknesses of O_2 plasma-treated Ir layers.
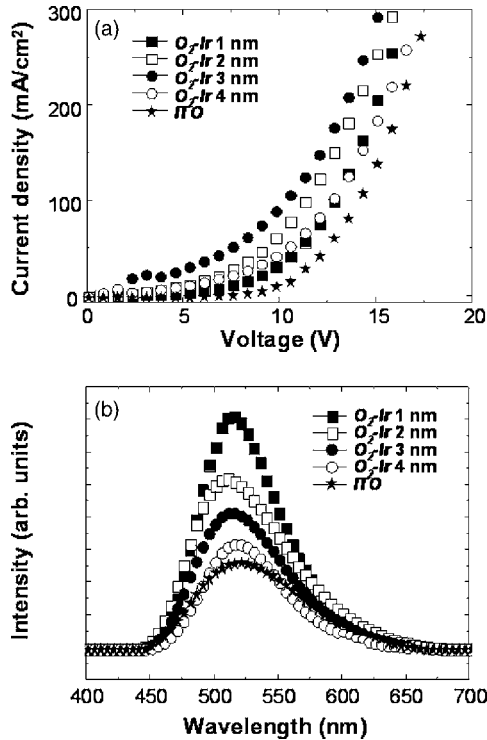

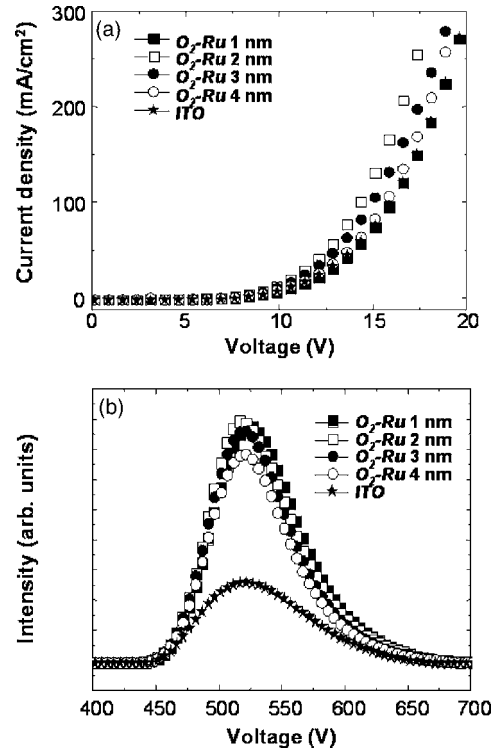FIG. 3. (a) Current-density voltage and (b) light output spectrum of OLEDs with different thicknesses of O_2 plasma-treated Ru layers.

thickness. It is considered that O_2-plasma-treated Ir layers are not completely transparent, decreasing the intensity as the Ir layer thickened. In considering the electrical and optical properties, Ir layers with a thickness of $1–2$ nm are optimum for obtaining high-performance devices.

The current-density-voltage curves as a function of different Ru layer thicknesses are displayed in Fig. 3(a). Devices using O_2-plasma-treated Ru layers show similar or better electrical properties than devices without Ru layers. In particular, OLEDs with 2-nm-thick Ru layers show an operation voltage of 14 V at the current density of 100 mA/cm^2, about 3 V lower than that for devices without Ru layers. Figure 3(b) presents the light output spectrum as a function of Ru layer thickness. The maximum intensity is also located at a wavelength of 520 nm. It was found that light output intensity decreased in proportion to Ru layer thickness. As the Ru layer thickened, the intensity of O_2-Ru/*ITO* decreased due to the opaque O_2-plasma-treated Ru layer. Therefore, we suggest that the optimum Ru layer thickness for obtaining high-performance devices is between 1 and 2 nm.

B. The change of SRPES spectra with O_2 plasma treatment

Figure 4(a) shows O 1s SRPES spectra of *ITO*, Ir/*ITO*, and O_2-Ir/*ITO* samples. In order to separate chemical bonding states, including those in the spectra, the spectral line shape was simulated using a suitable combination of Gaussian and Lorentzian functions. The O 1s peak separated into two components. The "P1" peak centered at 532.4 eV in *ITO* was due to residual surface contaminants.[15] The "P2" peak centered at 530.2 eV was assigned to O^{2-} ions in the tetra-

hedral interstices of face-centered-cubic In^{3+} ion arrays.[16] No change in the P1 peak intensity was found in Ir/*ITO*, but the P2 peak intensity was reduced. The photoemission flux I_d, which penetrated the film, decreased exponentially with the increase of thickness d, expressed as $I_d = I_o \exp(-d/\lambda)$, where I_o is the flux emitted by the clean backing material and λ is the inelastic mean free path of an electron traveling within a solid.[17] The reduction of P2 in the Ir/*ITO* is due to the exponential decrease of photoemission flux. In the O_2-Ir/*ITO* sample, a P3 peak centered at 531.3 eV appeared, indicating an O–Ir bond. Therefore, it is thought that the O_2 plasma treatment transformed the Ir layer into a transparent IrO$_x$ layer. The peak intensity of P1 decreased after O_2 plasma treatment, indicating reduction of residual surface contami-
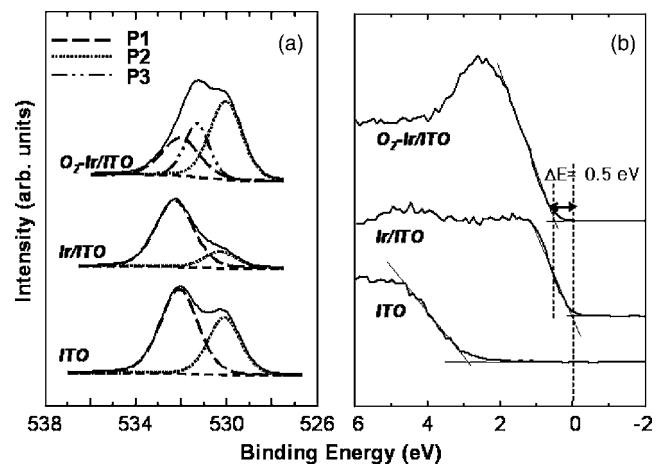

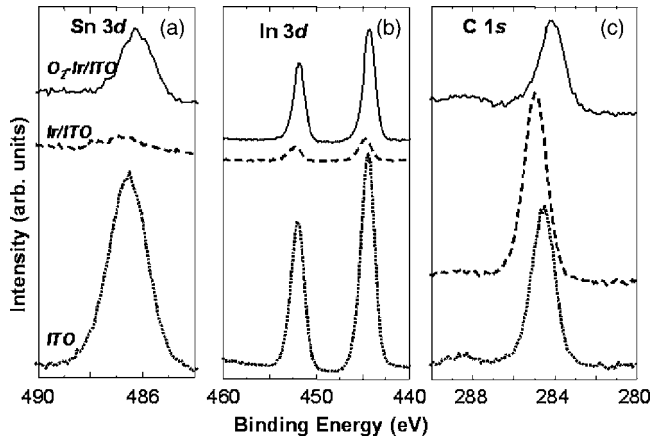FIG. 4. (a) O 1s and (b) valence-band spectra for *ITO*, Ir/*ITO*, and O_2-Ir/*ITO* samples.

FIG. 5. (a) Sn $3d$, (b) In $3d$, and (c) C $1s$ spectra for *ITO*, Ir/*ITO*, and O_2-Ir/*ITO* samples.

FIG. 6. (a) Ir $4f$ and (b) secondary electron emission spectra for *ITO*, Ir/*ITO*, and O_2-Ir/*ITO* samples.

nants. It seems that the peak intensity of P2 increased. But the P2/In calculated ratio from the integration of In $3d$ and O $1s$ spectra is almost identical in the Ir/*ITO* samples (P2/In =0.44) and O_2-Ir/*ITO* sample (P2/In=0.43). Therefore, it is thought that O_2 plasma treatment on the Ir layer did not affect the amount of O–In bonds, but only reduced the level of surface contaminants. The relative change in valence-band maximum (VBM) with the formation of IrO$_x$ layers is shown in Fig. 4(b). The VBM was calibrated with a clean Au surface. The VBM at the *ITO* surface is located 3.0 eV from the Fermi level. After the Ir layer was deposited on ITO surface, the Ir/*ITO* VBM coincided with the Fermi level, showing the metallic valance band. However, the VBM of O_2-Ir/*ITO* is located 0.5 eV from the Fermi level. This means that the band gap was produced due to the formation of IrO$_x$.

Figure 5 displays the (a) Sn $3d_{5/2}$, (b) In $3d$, and (c) C $1s$ core-level spectra of *ITO*, Ir/*ITO*, and O_2-Ir/*ITO* samples. After the deposition of Ir on ITO, the peak intensity of Sn $3d$ and In $3d$ decreased due to the exponential decrease of photoemission flux. After the O_2 plasma treatment of the Ir layer, peak intensity of Sn $3d$ and In $3d$ recovered and the intensity of C $1s$ decreased. It is thought that O_2 plasma treatment reduced the contents of contaminated carbon, increasing the photoemission flux of components.

The Ir $4f$ core-level spectra of Ir/*ITO* and O_2-Ir/*ITO* are shown in Fig. 6(a). The Ir $4f_{7/2}$ and Ir $4f_{5/2}$ peaks shifted about 1.5 eV toward a higher binding energy after O_2 plasma treatment. It is reported that the binding energy of Ir–O bond is higher than that of the Ir–Ir bond.[18] This result provides evidence for the formation of IrO$_x$ layers. The relative change of work function was measured using secondary electron emission spectra, as shown in Fig. 6(b). The onset of secondary electrons was determined by extrapolating two solid lines from the background and straight onset in the spectra.[19] The onset of secondary electrons for O_2-Ir/*ITO* shifted to the higher kinetic energy by 0.6 eV with respect to the onset for *ITO*. This result means that the work function of IrO$_x$-coated ITO is higher by 0.6 eV than that of O_2-plasma-treated ITO.

The O $1s$ SRPES spectra of *ITO*, Ru/*ITO*, and O_2-Ru/*ITO* are shown in Fig. 7(a). The O $1s$ peak is separated into two components, P1 and P2, using the same method in Fig.
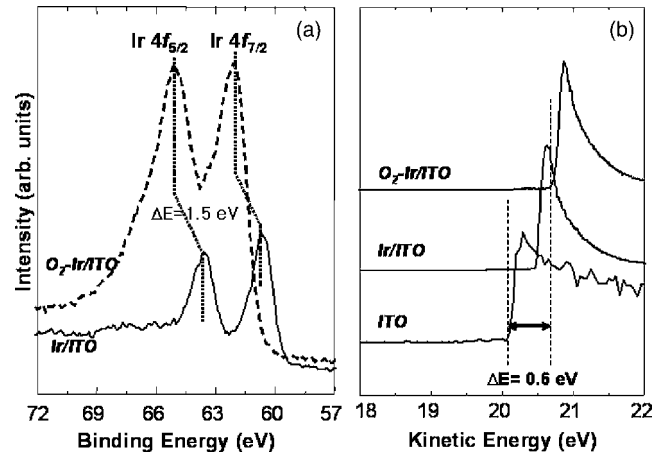
4. Overall peak intensity was reduced in Ru/*ITO* due to the exponential decrease of photoemission flux. In the O_2-Ru/*ITO* sample, a P3 peak centered at 531.1 eV appeared, indicating the O–Ru bond. Therefore, it is thought that the O_2 plasma treatment transformed the Ru layers into RuO$_x$ layers. The peak intensity of P1 decreased after O_2 plasma treatment of the Ru layers, indicating reduction of residual surface contaminants. Figure 7(b) shows the relative change in VBM with the formation of RuO$_x$ layers. After Ru layers were deposited on the ITO surface, the VBM shifted from 3.0 to 0 eV, indicating the disappearance of band gap. However, the VBM of O_2-Ru/*ITO* is located 2.2 eV from the Fermi level. This means that the band gap was produced due to the RuO$_x$ formation.

Figure 8 displays the (a) Sn $3d_{5/2}$ and (b) In $3d$ core-level spectra of *ITO*, Ru/*ITO*, and O_2-Ru/*ITO* samples. After the deposition of Ru on ITO, the peak intensity of Sn $3d$ and In $3d$ decreased due to the Ru layer thickness. After the O_2 plasma treatment, it seems that the peak intensity of Sn $3d$ and In $3d$ recovered. It is thought that the O_2 plasma treatment reduced the contents of contaminated carbon, thereby increasing the photoemission flux of components.
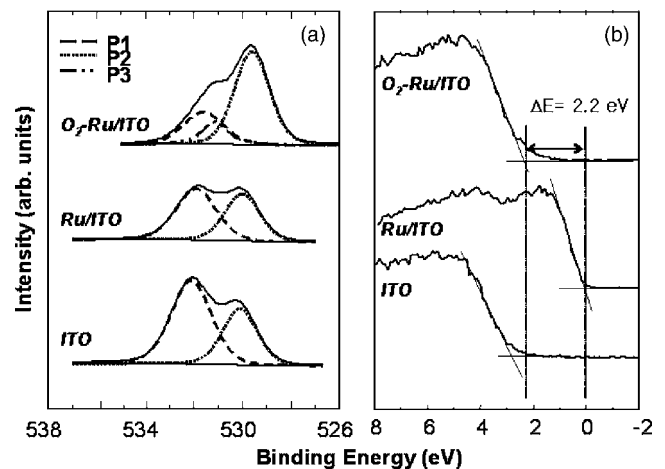

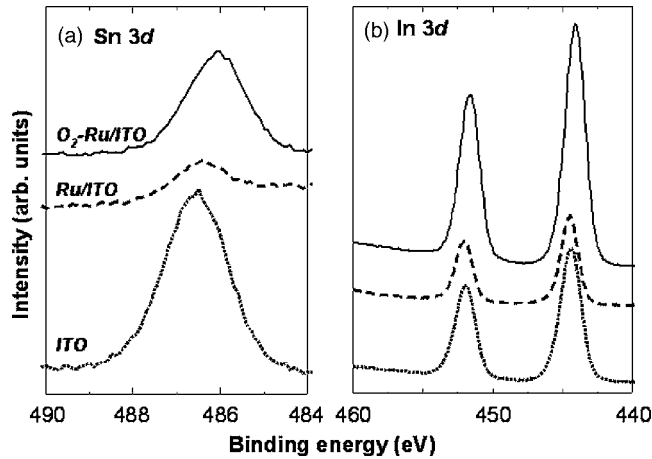FIG. 7. (a) O $1s$ and (b) valence-band spectra for *ITO*, Ru/*ITO*, and O_2-Ru/*ITO* samples.

FIG. 8. (a) Sn 3*d* and (b) In 3*d* spectra for *ITO*, Ru/*ITO*, and O$_2$-Ru/*ITO* samples.

FIG. 10. (Color online) AFM image of (a) *ITO*, (b) Ir/*ITO*, (c) O$_2$-Ir/*ITO*, (d) Ru/*ITO*, and (e) O$_2$-Ru/*ITO* samples.

The Ru 3*d* and C 1*s* core-level spectra of Ru/*ITO* and O$_2$-Ru/*ITO* are shown in Fig. 9(a). In the Ru/*ITO* sample, two peaks appeared at 280.5 eV indicating Ru 3$d_{5/2}$ and 284.6 eV indicating Ru 3$d_{3/2}$. The increase in peak intensity of Ru 3$d_{3/2}$ in comparison with that of Ru 3$d_{5/2}$ is due to the superimposition of the C 1*s* peak, because the difference in binding energy between the C 1*s* and Ru 3$d_{3/2}$ peaks is as low as 0.2 eV.[18] After the O$_2$ plasma treatment on the Ru layers, the Ru 3$d_{5/2}$ and Ru 3$d_{3/2}$ peaks shifted about 3.8 eV toward a higher binding energy and the peak intensity decreased. It has been reported that the binding energy of Ru–O bond is higher than that of the Ru–Ru bond.[18] The increase in peak intensity of Ru 3$d_{5/2}$ in comparison with that of Ru 3$d_{3/2}$ is due to the superimposition of the C 1*s* peak. This result provides evidence of the formation of RuO$_x$ layers. The relative change of work function was measured using secondary electron emission spectra, as shown in Fig. 9(b). The onset of secondary electrons was determined using the same method in Fig. 6(b). The onset of secondary electrons for O$_2$-Ru/*ITO* is located at the higher kinetic energy by 0.4 eV with respect to the onset for *ITO*. This result indicates that the work function of RuO$_x$-coated ITO is higher by 0.4 eV than that of the O$_2$-plasma-treated ITO.
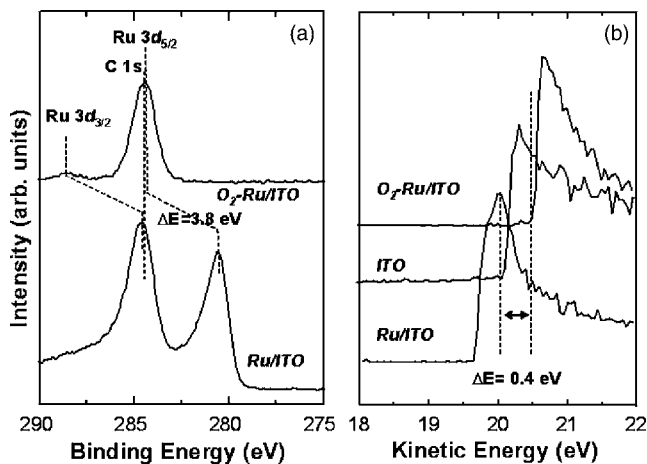
C. Surface analysis

The surface morphologies of (a) *ITO*, (b) Ir/*ITO*, (c) O$_2$-Ir/*ITO*, (d) Ru/*ITO*, and (e) O$_2$-Ru/*ITO* samples observed by AFM are shown in Fig. 10. The image size is 2 × 2 μm^2. The rms roughness was measured to be 4.6 Å for *ITO*, 4.7 Å for Ir/*ITO*, and 5.1 Å for Ru/*ITO*. After the O$_2$ plasma treatment, the rms roughness decreased to 4.5 Å for O$_2$-Ir/*ITO* and 4.7 Å for O$_2$-Ru/*ITO*. Therefore, it is thought that the O$_2$-plasma treatment reduced the surface roughness of transition-metal-coated ITO, suitable for HIL of OLEDs.

Figure 11 shows the x-ray reflectivity curves of Ir/*ITO*, O$_2$-Ir/*ITO*, Ru/*ITO*, and O$_2$-Ru/*ITO* samples. The density of the layer, layer thickness, and interface roughness could be extracted quantitatively after calculating the reflectivity with a computer algorithm based on the transfer-matrix method.[20] Here, we only discuss the amplitude of the oscillation of the reflectivity. The thicknesses of Ir and Ru layers estimated from the x-ray reflectivity data were 20 Å for Ir layers and 25 Å for Ru layers. After the O$_2$ plasma treatment, the thickness of the layers increased slightly to 21 Å for Ir and 28 Å for Ru layers. The film thickness is given by $2\pi/\Delta q$, where Δq is the period of the intensity oscillations in the reflectivity curves.[21] The oscillation amplitude decays exponentially as $\sim\exp[-\frac{1}{2}q_z^2(\sigma_1^2+\sigma_2^2)]$, where σ_1 is the roughness of the film surface and σ_2 is the roughness at the film/substrate interface.[21] Since the morphology at the film/substrate interface could not change during O$_2$ plasma treatment, the changes in oscillation amplitude represented
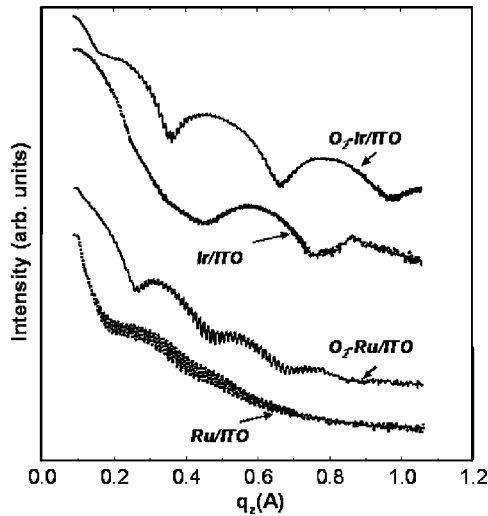

FIG. 9. (a) Ru 3*d* and (b) secondary electron emission spectra for *ITO*, Ru/*ITO*, and O$_2$-Ru/*ITO* samples.

FIG. 11. X-ray reflectivity data of Ir/*ITO*, O$_2$-Ir/*ITO*, Ru/*ITO* and O$_2$-Ru/*ITO* samples.

the evolution of the film surface. It is shown that the amplitude of the intensity oscillation increased after the O$_2$ plasma treatment on Ir and Ru layers. Therefore, it is thought that the Ir and Ru surface became smoother after O$_2$ plasma treatment.

IV. DISCUSSION

A. The effect of O$_2$ plasma treatment on Ir or Ru layers

After the Ir layers were treated by O$_2$ plasma, there were several changes in the SRPES spectra, such as the appearance of O–Ir bond in the O 1s spectrum, the shift of the Ir 4f peak toward a high binding energy, and the formation of band gap. Similar behavior was observed in the case of Ru layers, due to the phase transformation from Ir or Ru layers to IrO$_x$ or RuO$_x$. In addition, it was found in x-ray reflectivity measurements that the Ir and Ru surface became smoother after the O$_2$ plasma treatment. This is in good agreement with the previous report for platinum.[22] Since the Gibbs free energy changes per mole of oxygen in IrO$_x$ (ΔG_{300} =−188.049 kJ/mole) and RuO$_x$ (ΔG_{300}=−252.357 kJ/mole) are much lower than that in pure O$_2$ gas (ΔG_{300} =0 kJ/mole), the formation of oxides is more preferable under O$_2$ ambient.[23] The thicknesses of IrO$_x$ and RuO$_x$ were determined using the simple substrate-overlayer model of Eq. (1).[24]

$$d_{Ox} = \lambda \sin\theta \ln\left[\left(\frac{I_{Ox}}{I_{Me}}\right)\left(\frac{\rho_{Me}}{\rho_{Ox}}\right)+1\right]. \qquad (1)$$

In this equation, I_{Ox}/I_{Me} is the ratio of the Ir 4f (Ru 3d) peak area in the oxide layer to that in the metallic layer in SRPES spectra, θ is the takeoff angle (90°), d_{Ox} is the thickness of the oxide layer, and λ is the escape depth of Ir 4f (Ru 3d) photoelectrons, ρ_{Ox} and ρ_{Me} are the density of IrO$_x$ (RuO$_x$) and Ir (Ru), respectively. It was reported that the densities of Ir, IrO$_x$, Ru, and RuO$_x$ are 22.7, 11.7, 12.4, and 7.1 g/cm^3, respectively.[25] It is assumed that the escape depths of Ir 4f and Ru 3d photoelectrons through the oxide overlayer are
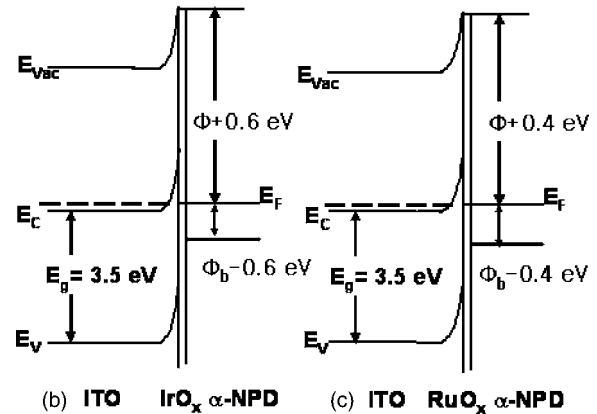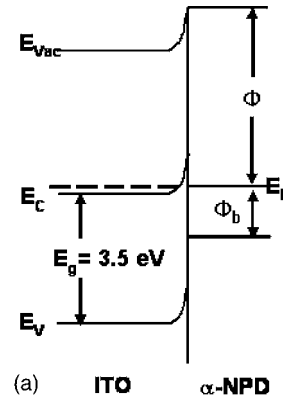

FIG. 12. Schematic band diagram: (a) O$_2$ plasma-treated ITO, (b) O$_2$ plasma-treated Ir layers on ITO, and (c) O$_2$ plasma-treated Ru layers on ITO.

identical to each other. Thus, the empirical Eq. (2) can be used.[24]

$$\lambda = 0.41a^{1.5}E^{0.5}. \qquad (2)$$

In this equation, E is the electron kinetic energy (in eV), and a is the diameter of the atoms (0.14 nm for Ir and 0.13 nm for Ru). Based on Eq. (2), λ was calculated to be 0.55 nm for Ir and 0.49 nm for Ru. Therefore, the thickness of the IrO$_x$ and RuO$_x$ was calculated to be 0.4 nm for Ir and 0.6 nm for Ru.

B. Change in electrical and optical properties of OLEDs

Based on these experimental observations, the reduction in operation voltage and the increase of luminance can be explained as below. The electron concentration of ITO is about 10^{20}–10^{21} cm^{-3}. Thus, the Fermi level of ITO is close to the conduction band maximum due to its high electron concentration. After the O$_2$ plasma treatment, surface band bending increased, as shown in Fig. 12(a). This is due to the formation of the Sn-deficient and O-rich surfaces by the treatment.[8] When the Ir (Ru) layer changed to a transparent IrO$_x$ (RuO$_x$) layer by O$_2$ plasma treatment, the work function increased, leading to the increase in band bending, as shown in Figs. 12(b) and 12(c). The injection barrier for holes from anodes to organic materials corresponds to the energy difference between the work function of anodes and ionization energy of organic materials. Thus, the hole injection barrier

of ITO, Φ_b, decreased to $\Phi_b=0.6$ eV in the O$_2$-Ir/*ITO* sample and decreased to $\Phi_b=0.4$ eV in the O$_2$-Ru/*ITO* sample. Thus, the interfacial layer of IrO$_x$ and RuO$_x$ plays a role in lowering the potential barrier between ITO and organic materials, reducing the turn-on voltage of OLEDs, and increasing internal quantum efficiency.

V. CONCLUSION

In conclusion, we have reported the advantage of interfacial transition-metal oxides, such as IrO$_x$ and RuO$_x$, between ITO anodes and hole transport layers of α-NPD on the electrical and optical properties of OLEDs. When the IrO$_x$ or RuO$_x$ layers are present between ITO and α-NPD, the operation voltage of OLEDs at the current density of 100 mA/cm^2 decreased from 17 to 11 V for the IrO$_x$ interlayers and from 17 to 14 V for the RuO$_x$ layers. The maximum luminance value increased from 1200 to 1800 cd/m^2 in OLEDs using IrO$_x$ and 2500 cd/m^2 in OLEDs using RuO$_x$. SRPES spectra revealed that Ir or Ru layers changed to IrO$_x$ or RuO$_x$ after O$_2$ plasma treatment. The oxide layer thickness produced by O$_2$ plasma treatment was estimated to be 0.4 nm for Ir layers and 0.6 nm for Ru layers. The oxide surface became smoother after O$_2$ plasma treatment. Furthermore, the work functions of IrO$_x$ and RuO$_x$ layers were higher by 0.6 and 0.4 eV than ITO, respectively. Thus, transition-metal oxide layers lowered the potential barrier for hole injection from ITO to α-NPD, reducing the turn-on voltage of OLEDs and increasing quantum efficiency.

ACKNOWLEDGMENTS

[1] H. Ishii, K. Sugiyama, E. Ito, and K. Seki, Adv. Mater. (Weinheim, Ger.) **8**, 605 (1999).
[2] D. R. Lide, *CRC Handbook of Chemistry and Physics*, 83rd ed. (CRC Press, Boca Raton, FL, 2002).
[3] S. E. Shaheen *et al.*, J. Appl. Phys. **84**, 2324 (1998).
[4] K. Tanaka, K. Maeda, and H. Usui, Appl. Phys. Lett. **81**, 3882 (2002).
[5] S. J. Kang, D. S. Park, S. Y. Kim, C. N. Whang, K. Jeong, and S. Im, Appl. Phys. Lett. **81**, 2581 (2002).
[6] Y. Q. Zhan *et al.*, Appl. Phys. Lett. **83**, 1656 (2003).
[7] R. B. H. Tahar, T. Ban, Y. Ohya, and Y. Takahashi, J. Appl. Phys. **83**, 2631 (1998).
[8] S. Y. Kim, K.-B. Kim, Y.-H. Tak, and J.-L. Lee, J. Appl. Phys. **95**, 2560 (2004).
[9] K. Sugiyama, H. Ishii, Y. Ouchi, and K. Seki, J. Appl. Phys. **86**, 1688 (1999).
[10] I.-M. Chan, W.-C. Cheng, and F. C. Hong, Appl. Phys. Lett. **80**, 13 (2002).
[11] I.-M. Chan, T.-Y. Hsu, and F. C. Hong, Appl. Phys. Lett. **81**, 1899 (2002).
[12] S. W. Tong, C. S. Lee, Y. Lifshitz, D. Q. Gao, and S. T. Lee, Appl. Phys. Lett. **84**, 4032 (2004).
[13] C.-M. Hsu and W.-T. Wu, Appl. Phys. Lett. **85**, 840 (2004).
[14] Y. T. Kim, C. W. Lee, and S. K. Kwak, Appl. Phys. A: Mater. Sci. Process. **67**, 807 (1995).
[15] L. Chkoda, C. Heske, M. Sokolowski, E. Umbach, F. Steuber, J. Staudigel, M. Stobel, and J. Simmerer, Synth. Met. **111**, 315 (2000).
[16] W. R. Salaneck, N. Johansson, K. Z. Xing, F. Cacialli, R. H. Friend, G. Beamson, and D. T. Clark, Synth. Met. **92**, 207 (1998).
[17] D. J. O'Connor, B. A. Sexton, and R. St. C. Smart, *Surface Analysis Methods in Materials Science* (Springer, Berlin, 1992).
[18] J. F. Moulder, W. F. Strickle, P. E. Sobol, and K. D. Bomben, *Handbook of X-ray Photoelectron Spectroscopy* (Perkin-Elmer, Eden Prairie, MN, 1992).
[19] J. M. Baik and J.-L. Lee, Met. Mater. Int. **10**, 555 (2004).
[20] L. G. Paratt, Phys. Rev. **95**, 359 (1954).
[21] D. Y. Noh, Y. Hwu, H. K. Kim, and M. Hong, Phys. Rev. B **51**, 4441 (1995).
[22] Z. Li, P. Beck, D. A. A. Ohlberg, D. R. Stewart, and R. S. Williams, Surf. Sci. **529**, 410 (2003).
[23] I. Barin, F. Sauert, E. S. Rhonhof, and W. S. Sheng, *Thermochemical Data of Pure Substances* (VCH, New York, 1989).
[24] D. Briggs and M. P. Seah, *Practical Surface Analysis: Auger and X-ray Photoelectron Spectroscopy* (Wiley, New York, 1990), Vol. 1.
[25] N. N. Greenwood and A. Earnshaw, *Chemistry of the Elements* (Dutterworth Heinemann, Oxford, 2001).